Malmquist, N.A.; Gujjar, R.; Rathod, P.K.; Phillips, M.A.: Analysis of flavin oxidation and electron-transfer inhibition in Plasmodium falciparum dihydroorotate dehydrogenase. Bioc…

ARTICLE *in* BIOCHEMISTRY · MARCH 2008

Impact Factor: 3.02 · DOI: 10.1021/bi702218c · Source: PubMed

4 AUTHORS, INCLUDING:

Ramesh Gujjar
organix,inc
9 PUBLICATIONS **340** CITATIONS
SEE PROFILE

Pradipsinh K Rathod
University of Washington Seattle
98 PUBLICATIONS **3,190** CITATIONS
SEE PROFILE

Margaret A Phillips
University of Texas Southwestern Medical Ce…
77 PUBLICATIONS **1,859** CITATIONS
SEE PROFILE

Published in final edited form as:
Biochemistry. 2008 February 26; 47(8): 2466–2475. doi:10.1021/bi702218c.

Analysis of Flavin Oxidation and Electron Transfer Inhibition in *Plasmodium falciparum* Dihydroorotate Dehydrogenase

Nicholas A. Malmquist[1], **Ramesh Gujjar**[2], **Pradipsinh K. Rathod**[2], and **Margaret A. Phillips**[1,*]

[1] Department of Pharmacology, University of Texas Southwestern Medical Center at Dallas, 6001 Forest Park Blvd, Dallas, Texas, 75390-9041

[2] Department of Chemistry and Pathobiology, University of Washington, Seattle, Washington 98195

Abstract

Plasmodium falciparum dihydroorotate dehydrogenase (*pf*DHODH) is a flavin-dependent mitochondrial enzyme that provides the only route to pyrimidine biosynthesis in the parasite. Clinically significant inhibitors of human DHODH (e.g. A77 1726) bind to a pocket on the opposite face of the flavin-cofactor from dihydroorotate (DHO). This pocket demonstrates considerable sequence variability, which has allowed species-specific inhibitors of the malarial enzyme to be identified. Ubiquinone (CoQ), the physiological oxidant in the reaction, has been postulated to bind this site despite a lack of structural evidence. To more clearly define the residues involved in CoQ binding and catalysis we undertook site-directed mutagenesis of seven residues in the structurally defined A77 1726 binding site, which we term the species-selective inhibitor site. Mutation of several of these residues (H185, F188 and F227) to Ala substantially decreased the affinity of *pf*DHODH specific inhibitors (40 – 240-fold). In contrast, only a modest increase in the K_m^{app} for CoQ was observed, though mutation of Y528 in particular caused a substantial reduction in k_{cat} (40 – 100-fold decrease). Pre-steady-state kinetic analysis by single wavelength stopped-flow spectroscopy showed that the mutations had no effect on the rate of the DHO-dependent reductive half-reaction, but most reduced the rate of the CoQ-dependent flavin oxidation step (3 – 20-fold decrease), while not significantly altering the K_d^{ox} for CoQ. As with the mutants, inhibitors that bind this site block the CoQ-dependent oxidative half-reaction without affecting the DHO-dependent step. These results identify residues involved in inhibitor binding and electron transfer to CoQ. Importantly, the data provide compelling evidence that the binding-sites for CoQ and species-selective site inhibitors do not overlap, and they suggest instead that inhibitors act either by blocking the electron path between flavin and CoQ, or by stabilizing a conformation that excludes CoQ binding.

Dihydroorotate dehydrogenase (DHODH) is a flavin-containing protein that catalyzes the conversion of dihydroorotate (DHO) to orotic acid (OA) in the fourth and only redox reaction in *de novo* pyrimidine biosynthesis. DHODH is classified into two families based upon amino acid sequence, substrate/cofactor dependence, and cellular localization (1). The cytosolic enzymes (Family 1) utilize fumarate or NAD^+ as the terminal electron acceptor (2), while the membrane bound enzymes (Family 2) transfer electrons to ubiquinone (CoQ) (Scheme 1), chemically coupling pyrimidine biosynthesis to the respiratory chain (3). Most gram-negative bacteria and many, but not all, eukaryotes have family 2 enzymes. This includes both malarial and human DHODH, which are localized to the inner membrane of the mitochondria. The Family 1A enzymes are thought to share a single binding-site for both DHO and fumarate

*Author to whom all correspondence should be addressed. Tel: (214) 645-6164. Fax: (214) 645-6166. Margaret.Phillips@UTSouthwestern.edu.

Supporting Information Available. CD spectra of wild-type and mutant *pf*DHODH. This material is available free of charge via the Internet at http://www.pubs.acs.org.

(4), while the Family 1B enzymes shuttle electrons from one side of the FMN through an adjacent [2Fe-2S] iron-sulfur cluster to a distant FAD prosthetic group (5). The Family 2 enzymes appear to have two distinct co-substrate binding-sites on either side of the FMN, consistent with the observed ping-pong kinetics (6–9).

DHODH is a validated drug target for the treatment of human disease. The active metabolite of the arthritis drug leflunomide (e.g. A77 1726; Figure 1) is a potent inhibitor of human DHODH (10). In the malarial parasite, *de novo* pyrimidine biosynthesis provides the only route to these essential metabolites, as the parasite is unable to scavenge preformed pyrimidines (11–13). Further, it has recently been demonstrated that the main role of the mitochondrial electron transport chain in the parasite is to provide oxidized CoQ to serve as an electron acceptor in the flavin oxidation step of the DHODH catalytic cycle (14). We previously identified a number of potent, species-selective inhibitors of *P. falciparum* DHODH by high-throughput screening, including N-(3,5-dichloro-phenyl)-2-methyl-3-nitro-benzamide (DCPMNB; Figure 1), and demonstrated that these inhibitors bind to the same site as A77 1726 by mutagenesis of the binding pocket (15). The structural basis for the observed species selectivity is evident through comparison of the x-ray structures of the human and malarial enzymes, which show that the A77 1726 binding-site is highly variable in amino acid sequence between the enzymes from the two species (Figure 2) (7,9,16). While both human and malarial structures contain A77 1726 in this site, A77 1726 is a poor inhibitor of the malarial enzyme (16). We therefore propose the nomenclature “species-selective inhibitor site” to describe this binding pocket.

Kinetic analysis of the inhibition patterns of both mammalian and *pf*DHODH have suggested that some, but not all, of the inhibitors that bind to the species-selective inhibitor site are competitive with CoQ (15,17–22). Brequinar and A77 1726 have been observed to bind to almost fully overlapping sites in the crystal structure of the human enzyme, yet non-competitive inhibition towards CoQ is observed for A77 1726 and competitive inhibition has been observed for brequinar (7,18). These results have led to the hypothesis that CoQ binds to the same (or an overlapping) site relative to A77 1726 and brequinar. However, because no structural data are available for CoQ bound to DHODH of any species, the location of the CoQ binding-site remains speculative and controversial.

The reductive half-reaction, where DHO is converted to OA, has been examined in considerable detail for both Family 1 and 2 enzymes by steady-state and pre-steady-state approaches (23–26). Further, this literature contains extensive data on the amino acid residues involved in the reaction at the DHO binding-site. In contrast, the oxidative half-reaction where FMN is re-oxidized by CoQ remains poorly studied. In order to provide insight into the position of the CoQ binding-site relative to inhibitors of *pf*DHODH we utilized site-directed mutagenesis of the species-selective inhibitor site and analyzed the effects of these mutations on both the steady-state reaction and the oxidative and reductive half-reactions which were monitored by pre-steady-state kinetic methods using single wavelength stopped-flow spectroscopy. The data provide insight into the residues involved in electron transfer between CoQ and FMN, and they suggest inhibitors bind in a channel that blocks the path of electron flow, but do not significantly overlap with the CoQ binding-site.

EXPERIMENTAL PROCEDURES

Materials

All buffers components, salts, and enzyme substrates were purchased from Sigma or were otherwise commercially available. Ni^{++}-NTA affinity resin was purchased from Qiagen. BL21-DE3 cells were from Novagen.

Synthesis of DHODH Inhibitors

Unless otherwise indicated, all anhydrous solvents were commercially obtained and stored under nitrogen. Reactions were performed under an atmosphere of dry nitrogen in oven-dried glassware and were monitored for completeness by thin layer chromatography (TLC) using silica gel 60 F-254 (0.25 mm) plates with detection with UV light. ^{1}H NMR spectra were recorded on dilute solutions in $CDCl_3$ or DMSO-d_6 at 300 MHz. Chemical shifts are reported in parts per million (δ) downfield from tetramethylsilane (TMS). Coupling constants (*J*) are reported in Hz. Electrospray ionization mass spectra were acquired on a Bruker Esquire Liquid Chromatograph-Ion Trap Mass Spectrometer. Flash chromatography was carried out with silica gel (32 – 63 μm). Melting points were taken in capillary tubes (Mel Temp apparatus) and are uncorrected.

N-(3,5-Dichloro-phenyl)-2-methyl-3-nitro-benzamide (DCPMNB) was prepared by the amidation of 2-methyl-3-nitro benzoic acid with 3,5-dichloro aniline. A catalytic amount of dimethylformamide (DMF) (2 – 4 drops) was added to a solution of 2-methyl-3-nitro-benzioc acid (0.905 g, 5 mmol) and oxalyl chloride (1.31 mL, 15 mmol) in CH_2Cl_2 (12 mL) at 0 – 5 °C, and the mixture was stirred for 15 hours under a N_2 atmosphere at room temperature. Following the removal of volatiles in vacuum, the resulting acid chloride was dissolved in tetrahydrofuran (THF) (20 mL) and added dropwise over period of 30 minutes to a stirred mixture of 3,5-dichloro aniline (0.972 g, 6 mmol) and triethyl amine (2.79 mL, 20 mmol) in THF (10 mL) maintained at 0 °C under N_2. The reaction mixture was allowed to warm to room temperature and then stirred for a further 3 hours. After removal of the THF evaporation in vacuum, the residue was partitioned between water (100 mL) and ethyl acetate (100 mL), and the separated aqueous layer washed with ethyl acetate (3 × 50 mL). The combined organic phase was washed with saturated aqueous NH_4Cl (100 mL) and brine (100 mL), and then dried ($MgSO_4$), filtered, and concentrated in vacuum to afford the crude product. Purification by flash chromatography using 20% ethyl acetate/hexane followed by $CH_2Cl_2/CH_3OH/NH_4OH$ (23:1:1) afforded the pure amide as a white solid (1 g, 67%). Melting point 171°C. ^{1}H NMR (300 MHz, DMSO-d_6): δ 8.03 (d, 1H, *J* = 7.5 Hz), 7.79–7.83 (m, 3H), 7.6 (t, 1H, *J* = 7.8 Hz), 7.38 (d, 1H, *J* = 1.5 Hz), 2.43 (s, 3H). MS *m*/*z* 325.1 ($M + H^+$).

A77 1726 was synthesized as previously described (16).

Plasmid Construction and Site Directed Mutagenesis

The previously described *pf*DHODH-pProEXHTa expression plasmid encoding amino acids 157 – 565 (16) was used as the cloning template. The *NdeI* restriction site at nucleotide 595 (full-length DHODH numbering) was eliminated using the QuickChange site-directed mutagenesis kit (Strategene) as recommended by the manufacturer, where the forward primer was 5′-GAAAATATAATATATTACC**C**TATGATACTAGTAATGATAGTATATATGC-3′ (altered base in bold). Next, *NdeI* and *XhoI* restriction sites were introduced by mutagenesis at the N and C-terminus of the *pf*DHODH ORF where the forward primer was, 5′-AACCTGTATTTT**CATATG**TTTTTTGAATCTTATAATCC-3′ and the reverse primer was 5′-CGTCGACCGTGT**CTCGAG**ACTTTTGCTATGCT-3′. The *NdeI-XhoI* DHODH fragment from the resulting plasmid was then subcloned into pET22b vector (Novagen) to generate the final expression construct (*pf*DHODH-pET22b-1). The *pf*DHODH ORF was sequenced in its entirety. Mutations of species-selective site residues to Ala were created using the QuickChange kit with the following primers (forward only are shown).

H185A	5′-GTGAAATATGT**GCT**GACCTTTTTTTATTACTAGG-3′
F188A	5′-GAAATATGTCATGACCTT**GCT**TTATTACTAGG-3′
F227A	5′-GGTGTTGCTGCAGGA**GCT**GATAAAAACGG-3′
R265A	5′-CCACGTATTTTT**GCA**GACGTTGAATCTAG-3′

I272A	5′-CGTTGAATCTAGAAGT**GCT**ATAAATTCATGTGG-3′
Y528A	5′-GGTGCTTCAGTTTGTCAATTA**GCT**TCTTGTTTGG-3′
Y528F	5′-CAGTTTGTCAATTA**TTT**TCTTGTTTGG-3′
Y528W	5′-CAGTTTGTCAATTA**TGG**TCTTGTTTGG-3′
L531A	5′-CAGTTTGTCAATTATATTCTTGT**GCG**GTTTTTAATGG-3′

P. falciparum DHODH Protein Expression and Purification

BL21-DE3 *E coli* cells containing the appropriate wild-type or mutant *pf*DHODH pET22b expression construct were grown in LB containing 100 mg/ml ampicillin overnight at 37°C. Large scale cultures (typically 6 liters) were inoculated with the overnight culture into LB broth with 10% glycerol and 100 mg/ml ampicillin and grown at 37°C to an OD_{600} of ~ 0.7. Protein expression was induced by the addition of isopropyl-beta-D-thiogalactopyranoside (IPTG; 200 μM), cultures were supplemented with FMN (100 μM) and grown at 16°C overnight. Cells were pelleted by centrifugation at 3000 × *g* at 4°C and the pellet re-suspended in 0.2 L lysis buffer (50 mM HEPES pH 8.0, 150 mM NaCl, 10 mM imidazole, 5 mM 2-mercaptoethanol, 100 μM FMN, 10% glycerol, and a protease inhibitor mixture consisting of phenylmethylsulfonyl fluoride (200 μM), leupeptin (1 μg/ml), antipain (2 μg/ml), benzamidine (10 μg/ml), pepstatin (1 μg/ml), and chymostatin (1 μg/ml)). Triton X-100 (2% v/v) and lysozyme (1 mg/ml) were added, and the mixture was stirred on ice for one hour before freezing in liquid nitrogen. DNase (0.05 mg/ml) was added to the thawed lysate, the mixture was sonicated on ice until cleared and centrifuged at 20000 × *g* at 4°C.

The resulting supernatant was loaded onto a Ni-NTA column equilibrated in buffer A (50 mM HEPES pH 8.0, 150 mM NaCl, 20 mM imidazole, 5 mM 2-mercaptoethanol, 100 μM FMN, 10% glycerol, 0.1% Triton X-100). The column was washed in buffer A until a stable baseline at A_{280} was reached, then bound enzyme was eluted with buffer B (50 mM HEPES pH 8.0, 150 mM NaCl, 300 mM imidazole, 5 mM 2-mercaptoethanol, 100 μM FMN, 10% glycerol, 0.1% Triton X-100). Fractions containing protein were pooled and concentrated with an Amicon Ultra centrifugal concentrating device (Amicon), desalted on a HiPrep 26/10 Desalting Column (Amersham Biosciences) equilibrated with enzyme assay buffer (50 mM HEPES pH 8.0, 150 mM NaCl, 10% glycerol, 0.1% Triton X-100) and re-concentrated as above.

Protein concentration was determined by Bradford analysis using bovine serum albumen as a standard. FMN concentration was determined by first heat denaturing the protein to release the bound cofactor (purified enzyme typically diluted to 1 – 20 μM), followed by measuring absorbance at 445 nm (ε_{445} = 12.5 mM^{-1} cm^{-1}) to calculate FMN concentration (27).

Circular Dichorism (CD) Spectroscopy

CD spectra were recorded for wild-type and mutant enzyme samples (8 μM protein) in 50 mM sodium phosphate pH 8.0. Spectra were collected from 190 to 260 nm using an Aviv CD Spectrometer Model 62DS at 25°C in quartz cuvettes (1 mm path length) with a five second integration time and three repetitions. Molar ellipticity data are presented as the average of the three readings versus buffer alone.

Steady-State Kinetic Analysis

Steady-state kinetic measurements were performed in enzyme assay buffer at 25°C and at 4° C. Production of orotic acid was observed directly at 296 nm (ε_{296} = 4.30 $mM^{-1}cm^{-1}$) when using both oxygen and ubiquinone analogs (CoQ_1, possessing a prenyl tail, or CoQ_D, possessing a decyl tail) as terminal electron acceptors. When ferricyanide was used as the electron acceptor, the reduction of ferricyanide was observed at 420 nm (ε_{420} = 1 mM^{-1} cm^{-1}), taking into consideration two moles of ferricyanide are reduced per every one mole of

DHO (4). For oxidase activity, DHO concentration (5 – 500 μM) was varied at a fixed enzyme concentration (100 nM). For CoQ and ferricyanide, assays were performed at a fixed concentration of DHO (0.5 mM), over a range of CoQ (1 – 100 μM) or ferricyanide (1 – 500 μM) concentrations in the presence of wild-type or mutant *pf*DHODH (5 – 50 nM). Oxygen was depleted from these reactions through the addition of 0.1 mg/ml glucose oxidase, 0.02 mg/ml catalase, and 50 mM glucose, followed by incubation for 5 min prior to assay. Data were fitted to the Michaelis-Menten equation to determine the steady-state parameters (k_{cat} and K_m).

Substrate-dependent DCPMNB inhibition experiments were performed with DHO (500 μM) and CoQ_1, CoQ_D, or ferricyanide (100 μM) or dissolved oxygen (~300 μM), 5 – 50 nM enzyme, and a range of inhibitor concentrations (10 nM – 100 μM). Wild-type and mutant *pf*DHODH IC_{50} values for DCPMNB were obtained from similar experiments using 500 μM DHO, 20 μM CoQ_D, 5 nM enzyme and a range of inhibitor concentrations (10 nM – 100 μM). Data were fitted to Equation 1 to determine the IC_{50}.

Pre-Steady-State Kinetic Analysis by Stopped Flow Spectroscopy

Rapid kinetic analysis was performed in enzyme assay buffer at 4°C on a Bio-Logic SFM-3 stopped flow instrument equipped with a 1 cm pathlength quartz cell, and controlled by BioKine 16 V 3.03 software. The calculated dead time was 4 ms at a flow rate of 15 ml/s. A wavelength of 485 nm was used to observe the transition of FMN between the oxidized and reduced state. For DHO-dependent reactions, enzyme (final concentration 20 μM) was mixed with a range of DHO concentration (final concentrations 63 – 1000 μM). CoQ_1-dependent experiments were performed under anaerobic conditions using the glucose oxidase and catalase system described above, as well as constant bubbling with nitrogen during sample preparation. For CoQ_1-dependent reactions, oxidized enzyme (45 μM) was reduced with a limiting amount of DHO (30 μM) under an atmosphere of nitrogen before loading on to the stopped flow instrument. Reduced enzyme (final concentration 10 μM) was then mixed with CoQ_1 (final concentrations 31 – 500 μM). A minimum of four reaction traces were recorded for each substrate concentration.

The observed DHO- and CoQ_1-dependent reactions were fitted to an exponential equation to obtain k_{obs} (Equation 2) (BioKine 16 software). Two exponentials were required to obtain good fits (as measured by the residual plots) to the DHO-dependent half-reactions, while the CoQ_1-dependent half-reaction was fitted to a single exponential. For the wild-type enzyme the residual plot for the CoQ_1-dependent half-reaction was not entirely non-random, however the deviation was small and random residuals were observed for the fit of the mutant enzymes, including for those with similar kinetic parameters to the wild-type enzyme. To avoid over fitting the data the wild-type data were also fitted to a single exponential. For both the DHO and CoQ_1-dependent half-reactions the resulting substrate-dependent fast phases ($k_{obs,1}$) displayed a hyperbolic dependence on substrate concentration and were fitted to Equation 3 to determine the $k_{red/ox}$ and K_d values for each half-reaction. These data were also fitted to an equation which accounts for a reversible reaction (28), but in all cases the reverse rate was found to be negligible or within the error of the analysis.

Inhibition experiments were performed by pre-mixing enzyme (10 or 20 μM final concentration, as above) and inhibitor at a concentration sufficient to ensure complete occupancy of the DHODH inhibitor binding-site (1 mM OA, 1 mM A77 1726, or 50 μM DCPMNB, final concentrations).

Molecular Modeling

The *pf*DHODH structure (1TV5.pdb) was displayed using the program PyMol (DeLano Scientific).

RESULTS

Analysis of the pfDHODH Species-selective Site

Residues in the species-selective inhibitor site within van der Waals distance of the inhibitor A77 1726 were identified in the x-ray structure of *pf*DHODH (Figure 1 and 2). In total, fifteen residues are found within 4 Å of A77 1726, and of these only five are conserved in sequence between human and *pf*DHODH. To identify residues that participate in the energetics of CoQ and inhibitor binding, five highly conserved residues (H185, F227, R265, Y528 and L531) and two variable residues (I272 and F188) were selected for analysis by Ala mutagenesis. F227, Y528 and L531 were selected because they make up an aromatic/hydrophobic patch that bridges between A77 1726 and the FMN cofactor. H185 and R265 were chosen because they are the only charged residues that contact the ligand, and I272 and F188 were selected to assess the role of residues that are variable between enzymes from different species. H185 also forms a bridging interaction between Y528 and F227. Site-directed mutagenesis was performed as described in Experimental Procedures, and the wild-type and mutant *pf*DHODH enzymes were expressed in *E. coli* and purified by Ni^{+2}-agarose column chromatography.

FMN Content of Wild-type and Mutant pfDHODH

The stochiometry of FMN to protein in the purified protein preparations was determined. FMN content ranged from 90 – 40% for wild-type enzyme and from 5 – 70% for the mutants. Mutation of F227, I272, Y528, and L531 to Ala affected the FMN content most, resulting in mutant enzymes with 5 – 25% FMN. Attempts to reconstitute FMN into enzyme preparations containing low FMN levels by unfolding and re-folding with various urea and/or guanidine concentrations in the presence of excess FMN were unsuccessful. The addition of free FMN to a reaction mixture containing FMN-poor enzyme did not result in an increase in catalytic rate. The CD spectra of the mutant enzymes were similar to the wild-type enzyme (Supplemental Figure S1), suggesting that the reduced flavin content does not result from gross mis-folding of the mutant enzymes. For kinetic analysis, enzyme concentration was determined by FMN concentration, thus normalizing for only catalytically competent enzyme.

Steady-state Kinetic Analysis of Wild-type and Mutant pfDHODH

Steady state kinetic analysis was performed on the wild-type and mutant enzymes in the presence of two ubiquinone analogues containing different length hydrophobic tails (CoQ_1 and CoQ_D (Table 1). CoQ_1 contains a single isoprenoid unit, while CoQ_D contains a longer aliphatic tail (Scheme 1). These two substrates were previously demonstrated to have different detergent micelle partitioning behavior, with CoQ_1 remaining soluble and CoQ_D partitioning into detergent micelles (29). Assays were performed in the presence of a glucose oxidase and catalase system to eliminate molecular oxygen from the reaction. For wild-type *pf*DHODH the measured kinetic constants (K_m^{app} CoQ 11 – 13 μM; k_{cat} 8 – 12 s^{-1}) were similar for the two substrates at 25°C. None of the Ala mutations had a significant effect on K_m^{app} for the CoQ substrate, with the largest affect (2 – 4-fold increase) being observed for the R265A mutation. A modest reduction in k_{cat} was observed for most of the mutations (2 – 4-fold). In contrast, mutation of Y528A caused a significant reduction in k_{cat} (40 – 100-fold respectively). Mutation of Y528 to Phe or Trp did not reduce the reaction rate as significantly as mutation to Ala, suggesting that an aromatic residue at this position plays a role in the reaction chemistry.

In the absence of CoQ substrates, molecular oxygen can function as the terminal electron acceptor to re-oxidize the FMN cofactor. The steady-state rates of this reaction were determined for dissolved O_2 present in buffers in the absence of the glucose oxidase and catalase system. Rates were determined for a range of DHO concentrations to determine the apparent k_{cat} for the oxidase reaction (0.42 s^{-1} for the wild-type enzyme). This rate is 25 – 30-fold lower than the CoQ catalyzed steady-state rate (Table 1). Only the I272A and Y528A mutant enzymes had oxidase rates that were significantly lower than the wild-type enzyme (5- and 4-fold lower, respectively). Since a single oxygen concentration was examined, these differences in the apparent k_{cat} for oxygen may reflect a change in the intrinsic k_{cat}, K_m, or both.

Steady-state kinetic inhibitor analysis

Previously, we identified DCPMNB as a potent and species-selective inhibitor of the malarial enzyme. DCPMNB showed competitive inhibition toward ubiquinone analogue substrates (15). Further, the effects of the H185A and R265A mutants on the binding of this inhibitor was characterized, leading to the conclusion that it bound to the species-selective inhibitor site. To extend these data we characterized the effect of the additional species-selective inhibitor site mutations on DCPMNB inhibition. DCPMNB inhibits the steady-state reaction in the presence of CoQ_1 or CoQ_D (100 μM) with an IC_{50} of 50 and 70 nM, respectively (Figure 3), while A77 1726 is a relatively weak inhibitor of *pf*DHODH (IC_{50} = 180 ± 3 μM). The IC_{50} for DCPMNB was substantially increased (40 – 240-fold) by three of the five tested mutations, confirming our prior conclusion that it binds to the structurally defined A77 1726 site (Table 2). We also examined the ability of DCPMNB to inhibit wild-type *pf*DHODH when the terminal electron acceptor is molecular oxygen or ferricyanide. Interestingly, in the presence of these inorganic oxidants, little inhibition was observed even at the highest concentration of DCPMNB tested (100 μM). These results demonstrate a lack of inhibition by DCPMNB when the steady-state reaction progresses in the presence of inorganic electron acceptors ferricyanide or oxygen, and they show that this inhibitor specifically blocks electron transfer to ubiquinone analogues.

The steady-state kinetic data demonstrate that mutation of species-selective inhibitor site significantly decreases inhibitor affinity for the enzyme, while having little to no effect on the K_m^{app} for CoQ. These data suggest that the CoQ binding-site may not overlap the inhibitor-binding site as previously suggested. However, because K_m is a reflection of multiple kinetic steps, and does not represent a true dissociation constant, effects on CoQ binding may be masked in the steady-state kinetic analysis. The finding that mutation of Y528 decreases the k_{cat} for the reaction suggests that this residue may play a catalytic role in the electron transfer between FMN and the oxidant. In order to determine more specifically which steps in the reaction pathway were being affected by the species-selective inhibitor site mutations, the reductive and oxidative half-reactions were characterized by pre-steady state kinetic analysis.

Pre-steady-state Kinetic Analysis of the FMN Reductive Half-reaction

Enzyme-bound oxidized FMN displays two characteristic absorbance bands that diminish upon reduction and re-appear at red-shifted positions in the presence of the reaction product orotic acid after re-oxidization (Figure 4). The DHO-dependent reduction of FMN was monitored by single wavelength stopped-flow spectroscopy at 485 nm, an isosbestic point of oxidized and re-oxidized FMN in the presence of product orotate. Data were collected in the absence of CoQ, thus only a single turnover was observed during the course of the experiment. The rate of the reaction was too fast to be measured at 25°C, the temperature of the steady-state analysis. Preliminary analysis demonstrated that most of the reaction occurred during the mixing dead time (4 ms) at this temperature. Data were collected at 4°C to slow the reaction and at this temperature approximately 50% of the reaction occurred in the dead time for the highest substrate concentration. Absorbance data were collected over a 4 – 1000 ms time period for a range of DHO concentrations (63 – 1000 μM) and were fitted to Equation 2 to determine the

observed rate constants for the reaction (k_{obs}). The data require two exponentials to obtain a good fit as demonstrated by the residual plots. The first observable kinetic phase ($k_{1,red}$) is dependent on DHO concentration and the data were fitted to Equation 3 to determine the kinetic constants for this phase of the reaction (for the wild-type enzyme $K_{d,red}$ = 230 μM; $k_{1,red}$ = 350 s^{-1}) (Table 3, Figure 5, Scheme 2). These data were also fitted to an equation which accounts for a reversible reaction (28), but in all cases the reverse rate was found to be near zero or within the error of the analysis. Estimating an extinction coefficient difference of $\Delta\varepsilon_{485}$ = 5 cm^{-1} mM^{-1} between oxidized and reduced enzyme, the amplitude change for this phase accounts for the reduction of approximately 80% of input enzyme, including the reaction that occurred during the mixing dead time. From these data it is clear that the DHO binding step occurs during the mixing dead time. The second kinetic phase displayed no clear dependence upon DHO concentration and $k_{2,red}$ ranged from 5 to 10 s^{-1} for the wild-type enzyme (Table 3 and Figure 5). These experiments were repeated for the mutant enzymes and similar results to the wild-type enzyme were obtained (Table 3). Thus, mutation of residues in the species-selective site has no significant effect on the reductive half-reaction catalyzed by *pf*DHODH.

The first observed kinetic step ($k_{1,red}$) is likely to represent the rate of the chemical step in which FMN is reduced and DHO is oxidized (Scheme 2). The second step could reflect several processes such as orotate release or a conformational change associated with its release, however, without additional data it is not possible to fully assign this step. Steady-state data were collected at 4°C for comparison, and at equivalent temperatures $k_{1,red}$ was significantly faster than the steady-state rate for both the wild-type and mutant enzymes. The $k_{2,red}$ was however similar in magnitude to k_{cat} for the wild-type enzyme, suggesting that this step is at least partially rate limiting (Table 3). For the mutant enzymes, $k_{2,red}$ is 3 – 6-fold slower than k_{cat}, with the exception of Y528A, where k_{cat} is 90-fold slower than $k_{2,red}$.

Pre-steady-state Kinetic Analysis of the FMN Oxidative Half-reaction

The oxidative half-reaction was also examined by single wavelength stopped-flow spectroscopy. Oxidized wild-type enzyme (45 μM) was reduced in anaerobic buffer by the addition of a limiting amount of DHO (30 μM) under an atmosphere of nitrogen before loading onto the stopped-flow instrument. Reduced enzyme (10 μM) was then mixed with CoQ_1 (31 – 500 μM), final concentrations. FMN oxidation was observed at 485 nm at 4°C over a time range of 4 – 500 ms (approximately ten half-lives of the slowest rate) and the resulting data were fitted to Equation 2. The data were fitted by a single exponential to obtain k_{obs} (Figure 6). This kinetic phase was dependent on CoQ_1 concentration and the k_{obs} data for the wild-type enzyme were fitted to Equation 3 (Table 3; $K_{d,ox}$ = 67 ± 5 μM; k_{ox} = 67 ± 2 s^{-1}). These data were also fitted to an equation which accounts for a reversible reaction (28), but in all cases the reverse rate was found to be negligible. The CoQ binding step occurred during the mixing dead time. The absorbance change of this phase suggests it reflects the chemical step for the conversion of FMN from the reduced to the oxidized state (Scheme 3). This rate at 4°C is 11-fold faster than the steady-state rate at 4°C (6.3 ± 0.3 s^{-1}), suggesting that this chemical step is not rate-limiting.

Analysis of the oxidative half-reaction by stopped-flow spectroscopy was undertaken for six of the species-selective site mutant enzymes (H185A, F188A, F227A, R265A, I272A, and Y528A). The mixing protocol and data collection were performed identically to the wild-type enzyme (as above). The data were best fitted to Equation 2 using a single exponential, and the resulting k_{obs} values were fitted to Equation 3 to determine the kinetic constants for the reaction (Table 3). The mutant enzymes tested exhibit a range of k_{ox} values, with H185A and Y528A displaying a 10 – 20-fold decrease in catalytic rate compared to wild-type enzyme, while the rates for F188A, F227A, and R265A were decreased by 2 – 9-fold. As with the wild-type

enzyme, k_{ox} is faster than the corresponding steady-state rates except for H185A, where the two rates are of similar magnitude (Table 3). Significantly, the mutant enzymes display little variation in $K_{d,ox}$ for CoQ_1 compared to wild-type enzyme. Mutation of the two charged residues within the species-selective site, H185 and R265, actually resulted in a two- to four-fold decrease, respectively, in K_d for CoQ_1, implying slightly tighter substrate binding to these mutant enzymes. These data show mutation of residues in the species-selective inhibitor site affect the rate of the CoQ dependent flavin oxidative half-reaction, but have little effect on the binding affinity of CoQ to the enzyme.

Effect of Inhibitors on the pfDHODH Oxidative and Reductive Half-reactions

The effect of A77 1726 and DCPMNB on the oxidative and reductive *pf*DHODH half-reactions was examined under saturating concentrations of each inhibitor using the rapid mixing protocols described above. For the DHO-dependent reductive half-reaction, neither inhibitor had a significant effect on the reaction, while orotic acid, the product of the reductive half-reaction, fully inhibited the reaction (Figure 7a). In contrast, when the CoQ_1-dependent oxidative half-reaction was examined, the reaction was fully inhibited by both A77 1726 and DCPMNB (Figure 7b), indicating that these inhibitors specifically block the CoQ_1-dependent oxidative half-reaction.

DISCUSSION

DHODH is an important drug target for the treatment of human rheumatoid arthritis, and a growing body of literature suggests that targeting the enzyme from the human malarial parasite may provide new chemotherapeutic approaches for this devastating human infection. Identified inhibitors (e.g. A77 1726) of both the human and parasite enzyme bind to a species-selective pocket adjacent to the FMN cofactor but on the opposite face from the DHO binding-site (7, 9). While the prevailing view has been that the physiological oxidant CoQ also binds this site, the available experimental evidence has not fully supported this hypothesis (18). In order to provide insight into the CoQ binding-site and the mechanism of both catalysis and inhibition, we characterized a series of mutations in the species-selective inhibitor site.

In contrast to the established hypothesis, our results suggest that the species-selective inhibitor site does not significantly overlap the CoQ binding-site. Prior studies reported that inhibitors bound to this site (e.g. brequinar, DCPMNB) were competitive inhibitors of CoQ substrates (15,18,20). However, we find that mutations in the site do not have significant effects on the K_m for the steady-state reaction nor on the DHO- or CoQ-dependent K_d values for the reductive or oxidative half-reactions. In contrast, mutation of H185, F188, or F227 significantly increases (60-, 40-, and 245-fold, respectively) the IC_{50} for DCPMNB, consistent with the hypothesis that this inhibitor binds the species-selective inhibitor site. Our data also show that the mutations reduce the rate of the CoQ-dependent oxidative half-reaction, without affecting the DHO-dependent reductive half-reaction. Similarly both A77 1726 and DCPMNB specifically block electron transfer between FMN and CoQ, but not oxidation by non-specific inorganic oxidants (O_2 or ferricyanide) that presumably are able to utilize alternative electron transfer paths. These results suggest that electron transfer from FMN occurs through one or more of the residues in the species-selective inhibitor site to CoQ bound at an alternative site. Inhibitors could act by either stabilizing a conformation of the enzyme that is unable to bind CoQ, or by preventing electron transfer. In the latter model, CoQ would prevent inhibitor binding in the channel (e.g. by blocking the channel entrance) while inhibitors would disrupt the electron transfer path between CoQ and FMN. Either of these models would yield competitive inhibition kinetics despite the lack of overlapping binding-sites.

Comparison of the steady-state and pre-steady state data provided insight into the rate-limiting step for the reaction catalyzed by *pf*DHODH. For the wild-type enzyme, the reductive half-

reaction was characterized by two observable kinetic steps. The first of these ($k_{1,red}$) was substantially faster than the steady-state rate and likely reflects the chemical reduction of FMN. The rate of the reductive half-reaction catalyzed by *pf*DHODH is comparable to that found for the Family 2 human and *E. coli* DHODH enzymes (23,24). Similarly, the single observable kinetic step for the oxidative half reaction was substantially faster than the steady-state rate, and is of a similar order of magnitude to the menadione-dependent oxidative half-reaction rate determined for the *E. coli* enzyme (23). Thus, neither the chemistry of FMN oxidation nor of reduction is likely to be rate-limiting for the steady-state reaction. In contrast to the substrate-dependent steps, the second observed phase ($k_{2,red}$) of the reductive half-reaction was significantly slower in rate, and for the wild-type enzyme and several of the mutants this rate is of similar magnitude to the steady-state rate. These data suggest that this step is at least partially rate determining. This step appears to occur after the chemical reduction of FMN by DHO, and is characterized by a relatively small absorbance change that may be a reflection of the rate of orotic acid release. However, this step could alternatively reflect a conformational change or other undefined step along the reaction coordinate, and additional experimental methods would be required to resolve this point.

The steady-state and rapid kinetics data presented here suggest that a number of residues in the species-selective inhibitor site play roles in the electron transfer step between FMN and CoQ. This conclusion is supported by the finding that the mutations affect the rate of the oxidative but not the reductive half-reaction. The rate constant for the CoQ dependent oxidative half reaction (k_{ox}) was decreased 10 – 20-fold for H185A and Y528A, and by 2 – 9-fold for F188A, F227A, and R265A. In the case of H185A, k_{ox} is of similar magnitude to the steady-state rate, suggesting the chemical oxidation of FMN has become rate-limiting for this mutant. Both k_{ox} and the steady-state rate were substantially reduced for Y528A compared to the wild-type enzyme. However, Y528 can be replaced by Phe or Trp without compromising the steady-state reaction rate, suggesting either the aromaticity or planarity of the side-chain, which stacks against the FMN cofactor, is important for electron transfer. While this hypothesis is supported by the data, it is also possible that for Y528A the electron transfer was disrupted due to a creation of a cavity in the active site. Y528 is invariant in the Family 2 DHODH enzymes and, consistent with our data, involvement of Y528 in either electron transfer or proton donation after electron transfer to ubiquinone substrates has been previously suggested (7,8).

The N-terminus of both human and *pf*DHODH is composed of outward-facing hydrophobic residues, which have been implicated in the partial burial of the CoQ binding-site into the mitochondrial membrane (7,9,29,30). This arrangement may allow natural and synthetic ubiquinone substrates to be positioned near the surface of the N-terminal domain, rather than deep within the species-selective inhibitor binding channel formed by the two N-terminal helices. Electrons could readily be channeled or tunneled from FMN to a distantly bound ubiquinone at the membrane surface through one or more of the residues within the species-selective inhibitor site. Electron transfer by tunneling through the protein backbone or the protein medium has been described for respiratory and photosynthetic enzymes, as has long distance hydrogen transfer (31–33). Additionally, long range electron transfer from FMN to a distant electron acceptor has been discussed previously for the *E coli* enzyme (23). Defining the exact route(s) of electron transfer would be greatly supported by a co-crystallized enzyme/CoQ substrate structure model.

Despite a large effort to understand the structure and mechanism of the CoQ-dependent family of DHODH enzymes, the binding-site for CoQ and the mechanism of electron transfer between this site and FMN have remained elusive. Our data clarify the relationship between the inhibitor binding-site and the CoQ binding-site, providing compelling evidence that these two sites are not overlapping. This finding provides important insight into the success of DHODH as a drug target in both mammalian and pathogen based disease processes. Potent inhibitors that bind

DHODH can be chemically distinct from either substrate (DHO or CoQ) since they do not share a common binding-site. Further, because the inhibitor binding-site does not overlap with substrate, it is less constrained to be conserved in amino acid sequence. Thus, the ability to isolate species-selective inhibitors of this target is a direct consequence of the reaction mechanism and the unusual mode of inhibition. These features are not commonly found in protein evolution and they suggest that DHODH is a particularly high value target for drug discovery.

EQUATIONS

$$v_i = \frac{v_o}{1 + \frac{[I]}{IC_{50}}} \quad \text{Equation 1}$$

$$A = \sum_{i=1}^{n} A_i e^{-k_{obs_i} t} + b \quad \text{Equation 2}$$

$$k_{obs} = \frac{k_1[S]}{K_d + [S]} \quad \text{Equation 3}$$

Supplementary Material

Refer to Web version on PubMed Central for supplementary material.

Acknowledgments

The authors thank Dr. Richard Auchus for informative discussions and careful review of the manuscript.

This work was supported by National Institutes of Health grants AI053680 (to MAP and PKR), and the Welch Foundation grant I-1257 (to MAP). NAM was supported in part by the Division of Basic Sciences Training Program Grant (NIH T32-MG00203).

ABBREVIATIONS

*pf*DHODH	*Plasmodium falciparum* dihydroorotate dehydrogenase
DHO	dihydroorotate
OA	orotic acid
FMN	flavin mononucleotide
NAD^+	nicotinamide adenine dinucleotide
CoQ	ubiquionone/co-enzyme-Q
CoQ_1	ubiquinone-1
CoQ_D	decylubiquinone
DCPMNB	*N*-(3,5-dichloro-phenyl)-2-methyl-3-nitro-benzamide
TLC	thin layer chromatography

DMSO	dimethyl sulfoxide
TMS	tetramethylsilane
DMF	dimethylformamide
THF	tetrahydrofuran
Ni^{++}-NTA	nickel-nitrilotriacetic acid
PQC	2-phenyl 5-quinolinecarboxylic acid

References

1. Nara T, Hshimoto T, Aoki T. Evolutionary implications of the mosaic pyrimidine-biosynthetic pathway in eukaryotes. Gene 2000;257:209–222. [PubMed: 11080587]
2. Nagy M, Lacroute F, Thomas D. Divergent evolution of pyrimidine biosynthesis between anaerobic and aerobic yeasts. Proc Natl Acad Sci U S A 1992;89:8966–8970. [PubMed: 1409592]
3. Jones ME. Pyrimidine nucleotide biosynthesis in animals: genes, enzymes, and regulation of UMP biosynthesis. Annu Rev Biochem 1980;49:253–279. [PubMed: 6105839]
4. Bjornberg O, Jordan DB, Palfey BA, Jensen KF. Dihydrooxonate is a substrate of dihydroorotate dehydrogenase (DHOD) providing evidence for involvement of cysteine and serine residues in base catalysis. Arch Biochem Biophys 2001;391:286–294. [PubMed: 11437361]
5. Marcinkeviciene J, Tinney LM, Wang KH, Rogers MJ, Copeland RA. Dihydroorotate dehydrogenase B of Enterococcus faecalis. Characterization and insights into chemical mechanism. Biochemistry 1999;38:13129–13137. [PubMed: 10529184]
6. Copeland RA, Davis JP, Dowling RL, Lombardo D, Murphy KB, Patterson TA. Recombinant human dihydroorotate dehydrogenase: expression, purification, and characterization of a catalytically functional truncated enzyme. Arch Biochem Biophys 1995;323:79–86. [PubMed: 7487077]
7. Liu S, Neidhardt EA, Grossman TH, Ocain T, Clardy J. Structures of human dihydroorotate dehydrogenase in complex with antiproliferative agents. Structure Fold Des 2000;8:25–33. [PubMed: 10673429]
8. Norager S, Jensen KF, Bjornberg O, Larsen S. E-coli dihydroorotate dehydrogenase reveals structural and functional distinctions between different classes of dihydroorotate dehydrogenases. Structure 2002;10:1211–1223. [PubMed: 12220493]
9. Hurt DE, Widom J, Clardy J. Structure of Plasmodium falciparum dihydroorotate dehydrogenase with a bound inhibitor. Acta Crystallogr D Biol Crystallogr 2006;62:312–323. [PubMed: 16510978]
10. Herrmann ML, Schleyerbach R, Kirschbaum BJ. Leflunomide: an immunomodulatory drug for the treatment of rheumatoid arthritis and other autoimmune diseases. Immunopharmacology 2000;47:273–289. [PubMed: 10878294]
11. Sherman IW. Biochemistry of Plasmodium (malarial parasites). Microbiol Rev 1979;43:453–495. [PubMed: 94424]
12. Gutteridge WE, Dave D, Richards WH. Conversion of dihydroorotate to orotate in parasitic protozoa. Biochim Biophys Acta 1979;582:390–401. [PubMed: 217438]
13. Rathod PK, Reyes P. Orotidylate-metabolizing enzymes of the human malarial parasite, Plasmodium falciparum, differ from host cell enzymes. J Biol Chem 1983;258:2852–2855. [PubMed: 6338005]
14. Painter HJ, Morrisey JM, Mather MW, Vaidya AB. Specific role of mitochondrial electron transport in blood-stage Plasmodium falciparum. Nature 2007;446:88–91. [PubMed: 17330044]
15. Baldwin J, Michnoff CH, Malmquist NA, White J, Roth MG, Rathod PK, Phillips MA. High-throughput screening for potent and selective inhibitors of Plasmodium falciparum dihydroorotate dehydrogenase. J Biol Chem 2005;280:21847–21853. [PubMed: 15795226]
16. Baldwin J, Farajallah AM, Malmquist NA, Rathod PK, Phillips MA. Malarial dihydroorotate dehydrogenase. Substrate and inhibitor specificity. J Biol Chem 2002;277:41827–41834. [PubMed: 12189151]

17. Davis JP, Cain GA, Pitts WJ, Magolda RL, Copeland RA. The immunosuppressive metabolite of leflunomide is a potent inhibitor of human dihydroorotate dehydrogenase. Biochemistry 1996;35:1270–1273. [PubMed: 8573583]
18. McLean JE, Neidhardt EA, Grossman TH, Hedstrom L. Multiple inhibitor analysis of the brequinar and leflunomide binding sites on human dihydroorotate dehydrogenase. Biochemistry 2001;40:2194–2200. [PubMed: 11329288]
19. Knecht W, Loffler M. Redoxal as a new lead structure for dihydroorotate dehydrogenase inhibitors: a kinetic study of the inhibition mechanism. FEBS Lett 2000;467:27–30. [PubMed: 10664450]
20. Knecht W, Loffler M. Species-related inhibition of human and rat dihydroorotate dehydrogenase by immunosuppressive isoxazol and cinchoninic acid derivatives. Biochem Pharmacol 1998;56:1259–1264. [PubMed: 9802339]
21. Hansen M, Le Nours J, Johansson E, Antal T, Ullrich A, Loffler M, Larsen S. Inhibitor binding in a class 2 dihydroorotate dehydrogenase causes variations in the membrane-associated N-terminal domain. Protein Sci 2004;13:1031–1042. [PubMed: 15044733]
22. Heikkila T, Thirumalairajan S, Davies M, Parsons MR, McConkey AG, Fishwick CW, Johnson AP. The first de novo designed inhibitors of Plasmodium falciparum dihydroorotate dehydrogenase. Bioorg Med Chem Lett 2006;16:88–92. [PubMed: 16236496]
23. Palfey BA, Bjornberg O, Jensen KF. Insight into the chemistry of flavin reduction and oxidation in Escherichia coli dihydroorotate dehydrogenase obtained by rapid reaction studies. Biochemistry 2001;40:4381–4390. [PubMed: 11284694]
24. Fagan RL, Nelson MN, Pagano PM, Palfey BA. Mechanism of flavin reduction in class 2 dihydroorotate dehydrogenases. Biochemistry 2006;45:14926–14932. [PubMed: 17154530]
25. Fagan RL, Jensen KF, Bjornberg O, Palfey BA. Mechanism of Flavin Reduction in the Class 1A Dihydroorotate Dehydrogenase from Lactococcus lactis. Biochemistry 2007;46:4028–4036. [PubMed: 17341096]
26. Combe JP, Basran J, Hothi P, Leys D, Rigby SE, Munro AW, Scrutton NS. Lys-D48 is required for charge stabilization, rapid flavin reduction, and internal electron transfer in the catalytic cycle of dihydroorotate dehydrogenase B of Lactococcus lactis. J Biol Chem 2006;281:17977–17988. [PubMed: 16624811]
27. Marcinkeviciene J, Jiang W, Locke G, Kopcho LM, Rogers MJ, Copeland RA. A second dihydroorotate dehydrogenase (Type A) of the human pathogen Enterococcus faecalis: expression, purification, and steady-state kinetic mechanism. Arch Biochem Biophys 2000;377:178–186. [PubMed: 10775458]
28. Strickland S, Palmer G, Massey V. Determination of dissociation constants and specific rate constants of enzyme-substrate (or protein-ligand) interactions from rapid reaction kinetic data. J Biol Chem 1975;250:4048–4052. [PubMed: 1126943]
29. Malmquist NA, Baldwin J, Phillips MA. Detergent-dependent kinetics of truncated Plasmodium falciparum dihydroorotate dehydrogenase. J Biol Chem 2007;282:12678–12686. [PubMed: 17329250]
30. Shi J, Palfey BA, Dertouzos J, Jensen KF, Gafni A, Steel D. Multiple states of the Tyr318Leu mutant of dihydroorotate dehydrogenase revealed by single-molecule kinetics. J Am Chem Soc 2004;126:6914–6922. [PubMed: 15174861]
31. Gray HB, Winkler JR. Electron tunneling through proteins. Quarterly reviews of biophysics 2003;36:341–372. [PubMed: 15029828]
32. Moser CC, Page CC, Dutton PL. Darwin at the molecular scale: selection and variance in electron tunnelling proteins including cytochrome c oxidase. Philosophical transactions of the Royal Society of London 2006;361:1295–1305. [PubMed: 16873117]
33. Sutcliffe MJ, Masgrau L, Roujeinikova A, Johannissen LO, Hothi P, Basran J, Ranaghan KE, Mulholland AJ, Leys D, Scrutton NS. Hydrogen tunnelling in enzyme-catalysed H-transfer reactions: flavoprotein and quinoprotein systems. Philosophical transactions of the Royal Society of London 2006;361:1375–1386. [PubMed: 16873125]

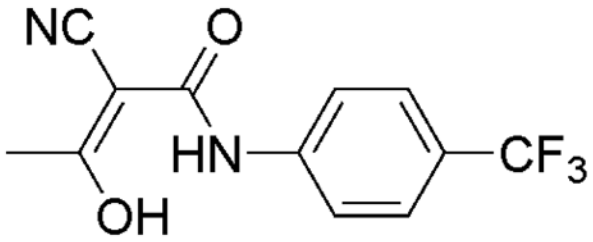

A77 1726

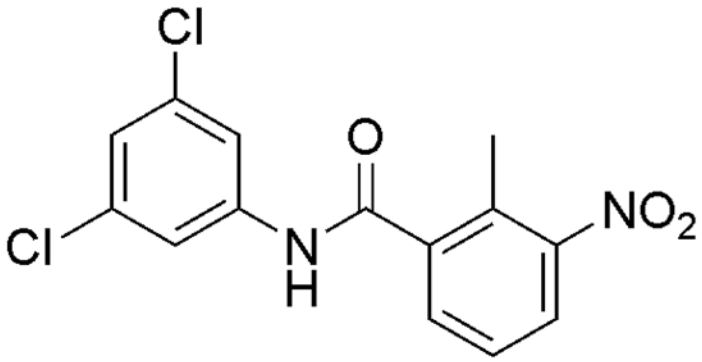

DCPMNB

Figure 1.
DHODH inhibitors.

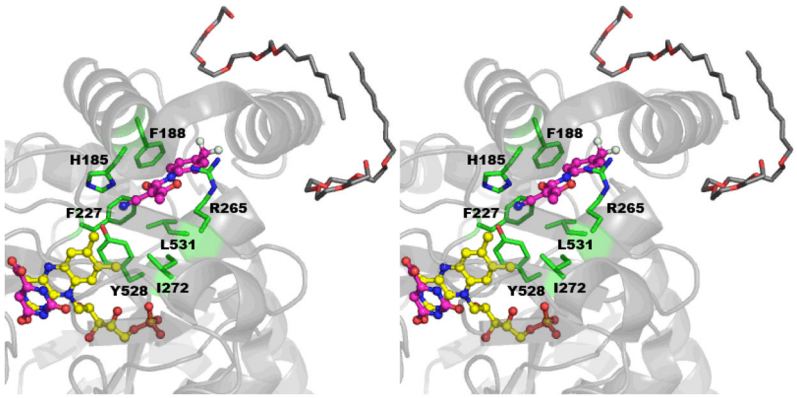

Figure 2. Species-selective inhibitor binding site of *pf*DHODH

A stereo cartoon drawing of the enzyme backbone bound to A77 1726 is displayed. The backbone is colored gray, oxygen is red, nitrogen blue, fluorine cyan, and phosphate orange. Carbon atoms of detergent molecules (pentaethylene glycol monooctyl ether) are gray, the inhibitor A77 1726 and product orotate are colored magenta, FMN is yellow, and residues within 4 Å of the inhibitor chosen for mutation are displayed and colored green. Residue F188 is an alanine and residue I272 is a valine in the human enzyme. All other residues displayed are conserved between the two species.

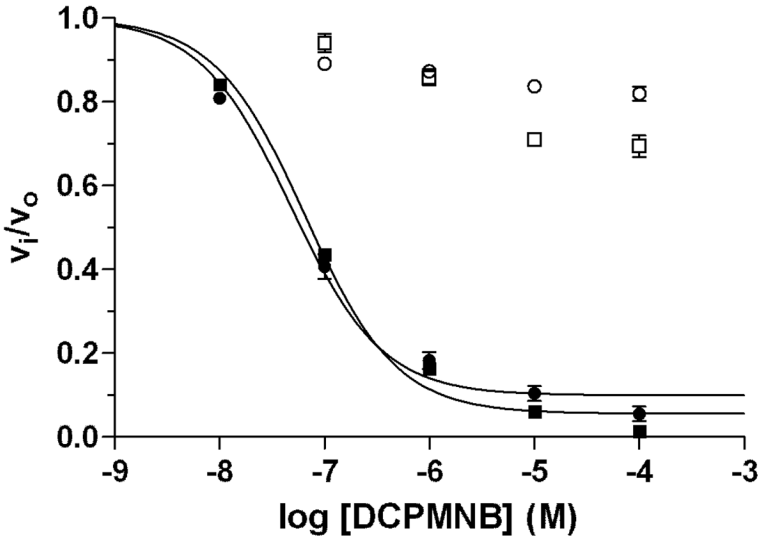

Figure 3. Inhibition of wild-type *pf*DHODH steady-state reaction by DCPMNB using different electron acceptors

The steady-state reaction was allowed to proceed in the presence of dissolved oxygen (~300 μM) (open circles) or $K_3Fe(CN)_6$ (100 μM) (open squares), CoQ_1 (100 μM) (closed circles), or CoQ_D (100 μM) (closed squares). DCPMNB inhibition data for CoQ_1 and CoQ_D yield an IC_{50} of 48 and 66 nM, respectively. DCPMNB (100 μM) inhibits oxygen- and $K_3Fe(CN)_6$-dependent activity by 12% and 30% respectively.

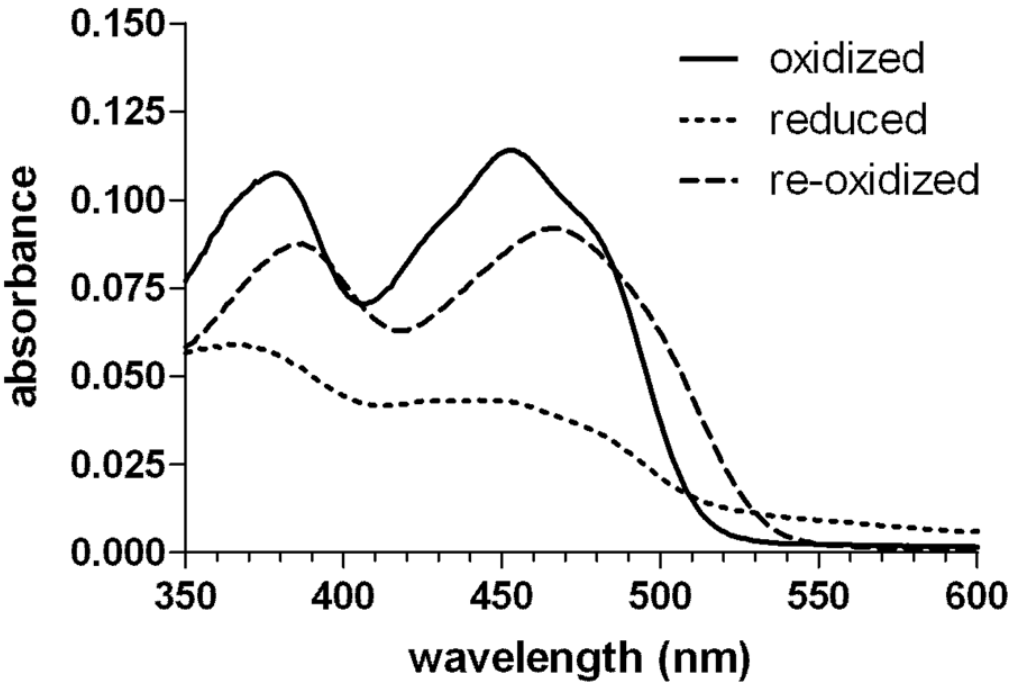

Figure 4. Absorbance spectra of wild-type *pf*DHODH

Oxidized *pf*DHODH (10 μM) in the presence of buffer containing dissolved oxygen (solid line). *pf*DHODH was mixed with DHO (500 μM) and the spectra of the reduced enzyme was recorded immediately (dotted line). The reaction with DHO and dissolved oxygen was allowed to proceed for several minutes to completion and the absorbance spectrum of re-oxidized enzyme, in the presence of product orotate, was recorded (dashed line).

a)

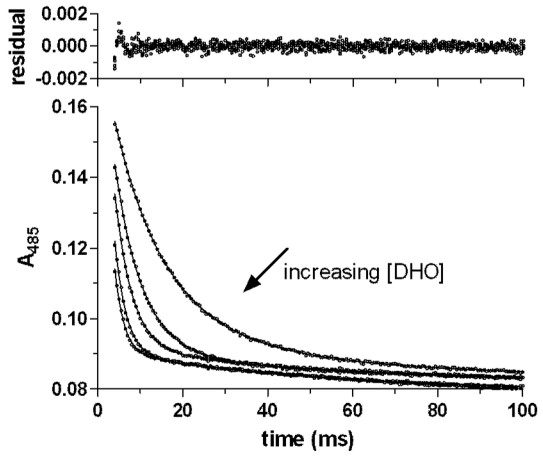

b)

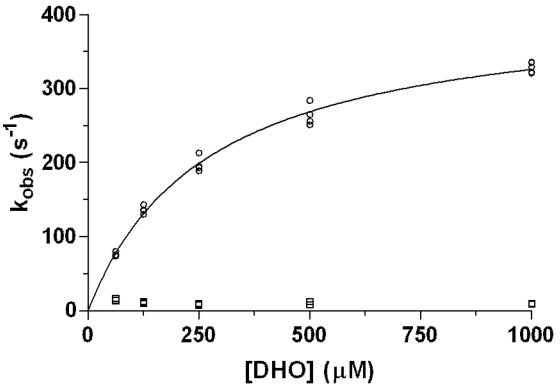

Figure 5. Pre-steady-state kinetic analysis of the wild-type *pf*DHODH reductive half-reaction

(a) Absorbance traces (closed circles) for *pf*DHODH (final concentration 20 μM) after rapid mixing with DHO (final concentrations 62, 125, 250, 500, 1000 μM) at 4°C. Data were fitted to Equation 2 using double exponentials (solid curves) to obtain k_{obs} values. The residual plot for the fit are displayed above the graph. (b) The DHO concentration dependence of $k_{obs,1}$ and $k_{obs,2}$ (open circles and open squares, respectively). The $k_{obs,1}$ for the first observed kinetic step was fitted to Equation 3 ($K_{d,red}$ = 230 ± 70 μM; $k_{1,red}$ = 350 ± 30 s^{-1}).

a)

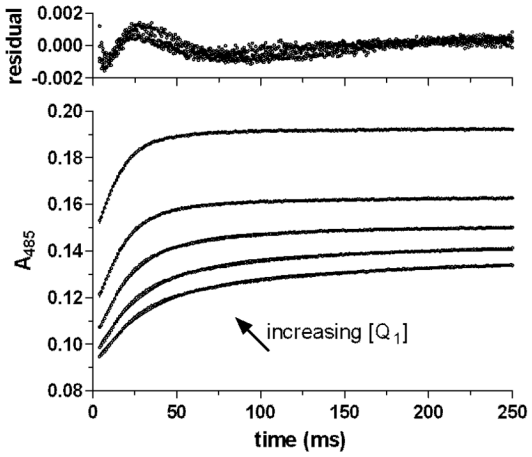

b)

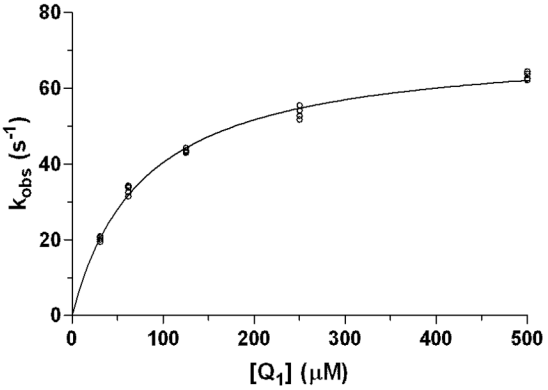

Figure 6. Pre-steady-state kinetic analysis of the wild-type *pf*DHODH oxidative half-reaction

(a) Absorbance traces (closed circles) are displayed for enzyme (15 μM enzyme pre-reduced with 10 μM DHO, final concentrations) after rapid mixing with CoQ_1 (final concentrations 31, 62, 125, 250, 500 μM) at 4°C. Data were fitted to Equation 2 using a single exponential (solid curve). The residual plot for the fit are displayed above the graph. (b) CoQ_1 concentration dependence of the $k_{obs,1}$ (open circles). The k_{obs} for the observed kinetic step was fitted to the Equation 3 to determine the kinetic parameters ($K_{d,ox}$ = 67 ± 5 μM; $k_{1,ox}$ = 67 ± 2 s^{-1}).

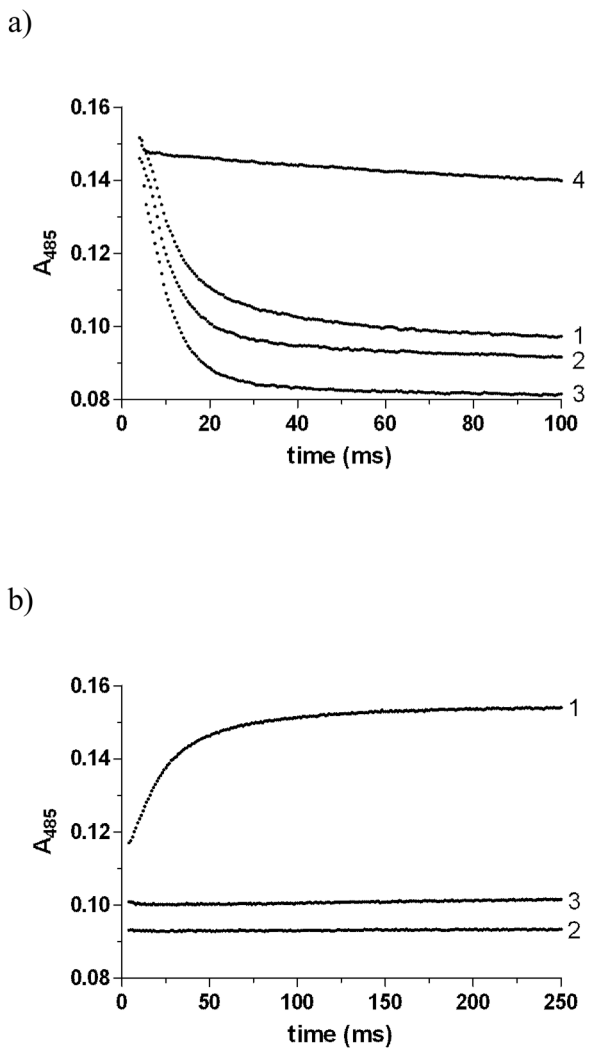

Figure 7. Pre-steady-state kinetic analysis of wild-type *pf*DHODH in the presence of inhibitors

Reductive half-reaction: (a) Absorbance traces of enzyme (20 μM) alone (trace 1) or pre-mixed with DCPMNB (50 μM) (trace 2), A77 1726 (1 mM) (trace 3), or OA (1 mM) (trace 4) and then mixed with DHO (125 μM). All concentrations are after mixing. Oxidative half-reaction: (b) Absorbance traces of enzyme (15 μM pre-reduced with 10 μM DHO) alone (trace 1) or pre-mixed with DCPMNB (50 μM) (trace 2) or A77 1726 (1 mM) (trace 3) and then mixed with CoQ_1 (100 μM). All concentrations are after mixing. Experiments were performed at 4° C.

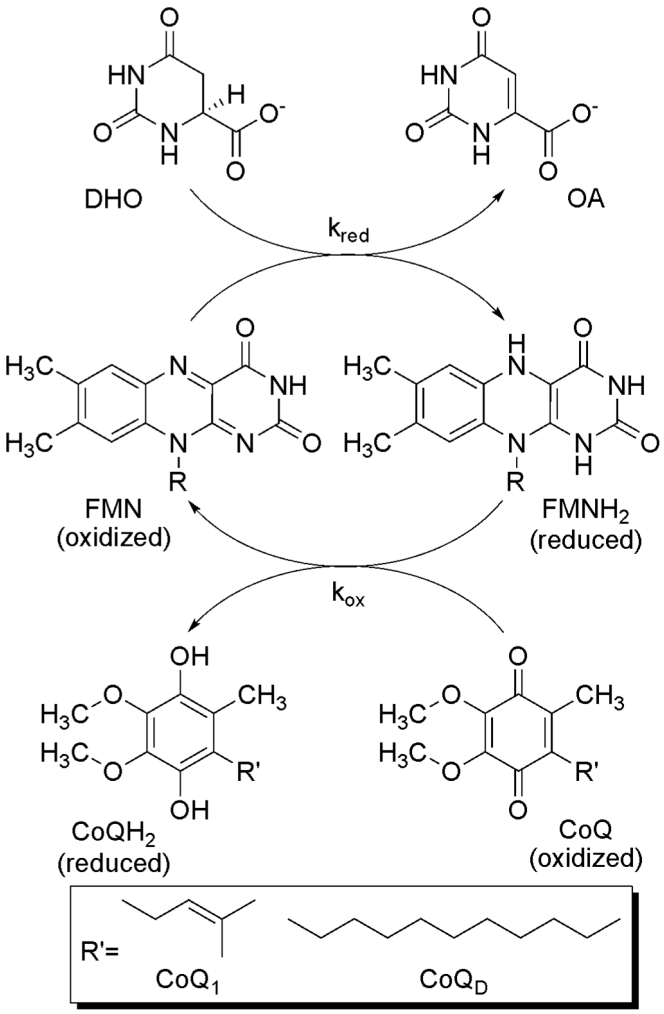

Scheme 1.

$$E_{ox} + DHO \overset{K_{d,red}}{\rightleftharpoons} E_{ox}\text{-}DHO \underset{(fast)}{\overset{k_{1,red}}{\rightleftharpoons}} E_{red}\text{-}OA \underset{(slow)}{\overset{k_{2,red}}{\rightleftharpoons}} E_{red}\sim OA$$

Scheme 2.

$$E_{red} + CoQ \overset{K_{d,ox}}{\rightleftharpoons} E_{red}\text{-}CoQ \overset{k_{ox}}{\rightleftharpoons} E_{ox}\text{-}CoQH_2$$

Scheme 3.

Table 1

Steady-state kinetic parameters of wild-type and mutant *pf*DHODH

Steady-state experiments were performed at 25°C. Values for k_{cat} (or k_{cat}^{app}) and K_m^{app} for a variety of electron acceptors were derived as described in the text. Errors represent the standard error of the fit for at least two determinations.

	O_2	Q_1		Q_D	
***pf*DHODH**	**k_{cat}^{app} (s^{-1})**	**K_m^{app} (μM)**	**k_{cat} (s^{-1})**	**K_m^{app} (μM)**	**k_{cat} (s^{-1})**
wt	0.42 ± 0.01	11 ± 2	7.8 ± 0.3	13 ± 1	12 ± 1
H185A	0.57 ± 0.04	22 ± 3	7.3 ± 2.2	34 ± 9	7.9 ± 3.3
F188A	0.53 ± 0.03	15 ± 3	2.6 ± 0.4	20 ± 3	4.3 ± 0.2
F227A	0.43 ± 0.05	16 ± 2	2.6 ± 0.1	20 ± 3	3.5 ± 0.2
R265A	0.44 ± 0.02	38 ± 3	3.1 ± 0.1	26 ± 1	5.0 ± 0.1
I272A	0.083 ± 0.004	7.8 ± 0.4	1.5 ± 0.1	12 ± 1	1.8 ± 0.1
Y528A	0.10 ± 0.01	16 ± 3	0.19 ± 0.03	8.8 ± 2.3	0.12 ± 0.01
Y528F	0.63 ± 0.03	20 ± 3	1.9 ± 0.1	53 ± 4	1.2 ± 0.1
Y528W	0.18 ± 0.01	48 ± 14	5.1 ± 0.6	45 ± 11	6.8 ± 0.7
L531A	0.25 ± 0.02	17 ± 2	5.1 ± 0.9	16 ± 1	8.6 ± 1.4

Table 2

IC_{50} values for *pf*DHODH inhibition by DCPMNB

Inhibition was examined in the presence of 500 μM DHO and 20 μM CoQ_D using 5 nM enzyme. Errors represent the standard error of the fit.

*pf*DHODH	IC_{50} DCPMNB
wt	49 ± 1
H185A	2900 ± 100
F188A	1900 ± 100
F227A	12000 ± 1000
R265A	100 ± 10
L531A	87 ± 1

Table 3

Pre-steady-state kinetic analysis of wild-type and mutant *pf*DHODH

Pre-steady-state experiments were performed at 4°C using CoQ_1 as a substrate; CoQ_1-depedent steady state data were also collected at 4°C to allow direct comparison. Values for K_d and $k_{red/ox}$ were derived as described in the text. Errors represent the standard error of the fit.

	steady-state reaction		reductive half-reaction			oxidative half-reaction	
***pf*DHODH**	K_m^{app} (μM)	k_{cat} (s^{-1})	$K_{d,red}$ (μM)	$k_{1,red}$ (s^{-1})	$k_{2,red}$ (s^{-1})	$K_{d,ox}$ (μM)	k_{ox} (s^{-1})
wt	16 ± 2	6.3 ± 0.3	230 ± 70	350 ± 30	8.2 ± 0.4	67 ± 5	67 ± 2
H185A	41 ± 5	2.3 ± 0.1	98 ± 42	180 ± 10	9.9 ± 1.6	32 ± 3	2.8 ± 0.1
F188A	26 ± 2	2.8 ± 0.1	100 ± 20	180 ± 10	5.7 ± 0.5	74 ± 3	16 ± 1
F227A	18 ± 1	1.7 ± 0.1	120 ± 10	180 ± 10	6.2 ± 0.6	90 ± 9	26 ± 1
R265A	21 ± 3	1.7 ± 0.1	78 ± 8	200 ± 10	8.0 ± 0.7	14 ± 1	7.4 ± 0.1
I272A	15 ± 2	1.1 ± 0.1	94 ± 28	210 ± 20	6.4 ± 0.7	87 ± 6	77 ± 2
Y528A	37 ± 5	0.10 ± 0.01	70 ± 29	200 ± 10	8.7 ± 0.7	51 ± 5	2.9 ± 0.1
L531A	nd	nd	150 ± 10	300 ± 10	7.4 ± 1.2	nd	nd